limited amount of work in eukaryotes, it appears that the heat shock proteins, and in particular the hsp70 members, serve functions during normal cell growth and in cells subjected to stress. Our results indicate that functional 70K hsps are required for mammalian cells to survive conditions of brief, but severe, heat shock treatment. It has been suggested that, because of their relatively high abundance in normal and stressed cells, their intracellular localization, and their ability to bind and perhaps hydrolyze adenosine triphosphate (ATP) the 70K hsps might serve a general role in stabilizing proteins against denaturation or in promoting the renaturation of proteins in cells that have been exposed to protein denaturing (stress) agents (*6, 7, 21*). This role could be fulfilled by an unfoldase activity similar to that proposed for a constitutively produced member of the hsp70 family in the transport of different protein species across intracellular membranes during normal cell growth (*16*). These experiments, as well as those presented in (*26*), provide strong evidence that the activity of hsp70 is required for the survival of cells during and after thermal stress.

REFERENCES AND NOTES

1. E. A. Craig, *CRC Crit. Rev. Biochem.* **18**, 239 (1985).
2. S. Lindquist, *Annu. Rev. Biochem.* **55**, 1151 (1986).
3. W. J. Welch and J. R. Feramisco, *J. Biol. Chem.* **257**, 14949 (1982).
4. ———, *ibid.* **259**, 4501 (1984).
5. J. M. Velazquez and S. Lindquist, *Cell* **36**, 655 (1984).
6. M. J. Lewis and H. R. Pelham, *EMBO J.* **4**, 3137 (1985).
7. W. J. Welch and J. P. Suhan, *J. Cell Biol.* **103**, 2035 (1986).
8. E. W. Gerner and M. J. Scheider, *Nature* **256**, 500 (1975).
9. J. Plesset, C. Palm, C. S. McLaughlin, *Biochem. Biophys. Res. Commun.* **108**, 1340 (1982).
10. G. C. Li and Z. Werb, *Proc. Natl. Acad. Sci. U.S.A.* **79**, 3218 (1982).
11. J. Landry *et al.*, *Cancer Res.* **42**, 2457 (1982).
12. J. R. Subjeck, J. J. Sciandra, R. J. Johnson, *Br. J. Radiol.* **55**, 579 (1982).
13. G. C. Li and A. Laszlo, *J. Cell. Physiol.* **122**, 91 (1985).
14. E. Craig and K. Jacobsen, *Cell* **38**, 841 (1984).
15. H. Saito and H. Uchida, *J. Mol. Biol.* **113**, 1 (1977).
16. R. J. Deshaies, B. D. Koch, M. Werner-Washburne, E. A. Craig, R. Schekman, *Nature* **332**, 800 (1988); W. J. Chirico, M. G. Waters, G. Blobel, *ibid.*, p. 805.
17. J. J. C. Lin and K. Burridge, *J. Cell Biol.* **87**, 216 (1980).
18. W. J. Welch and J. F. Feramisco, *Mol. Cell Biol.* **5**, 1571 (1985).
19. K. T. Riabowol, R. J. Vosatka, E. B. Ziff, N. J. Lamb, J. R. Feramisco, *ibid.* **8**, 1670 (1988); K. Riabowol, unpublished data.
20. W. J. Welch, J. I. Garrels, G. P. Thomas, J. J. C. Lin, J. R. Feramisco, *J. Biol. Chem.* **258**, 7102 (1983).
21. L. A. Mizzen and W. J. Welch, *J. Cell Biol.* **106**, 1105 (1988).
22. K. T. Riabowol, unpublished data.
23. K. H. Antman and D. M. Livingston, *Cell* **19**, 627 (1980).
24. W. E. Mercer, D. Nelson, J. K. Hyland, C. M. Croce, R. Baserga, *Virology* **127**, 149 (1983).
25. L. S. Mulcahy, M. R. Smith, D. W. Stacey, *Nature* **313**, 241 (1985).
26. R. N. Johnston and B. L. Kucey, *Science*, in press.
27. K. T. Riabowol, *Anal. Biochem.*, in press.

28. We thank M. Zoller for the gift of antibodies directed against the catalytic subunit of yeast cAMP-dependent protein kinase. Supported by an NIH general medical grant to W.J.W. (GM33551). K.R. was supported by an NIH training grant fellowship, an American Heart Association fellowship (Nassau County chapter), and an NIH-PHS grant awarded to J. Feramisco. L.M. was supported by a Medical Research Council (Canada) postdoctoral fellowship.

29 June 1988; accepted 29 August 1988

Parallel Integration of Vision Modules

T. POGGIO, E. B. GAMBLE, J. J. LITTLE

Computer algorithms have been developed for several early vision processes, such as edge detection, stereopsis, motion, texture, and color, that give separate cues to the distance from the viewer of three-dimensional surfaces, their shape, and their material properties. Not surprisingly, biological vision systems still greatly outperform computer vision programs. One of the keys to the reliability, flexibility, and robustness of biological vision systems is their ability to integrate several visual cues. A computational technique for integrating different visual cues has now been developed and implemented with encouraging results on a parallel supercomputer.

ALTHOUGH IT IS REASONABLE THAT combining the evidence provided by multiple visual cues—for example, edge detection, stereo, and color—should provide a more reliable map of the objects in a visual scene than any single cue alone, it is not obvious how to accomplish this integration. One of the most important constraints for recovering surface properties from each of the individual cues is that the physical processes underlying image formation, such as depth, orientation, and reflectance of the surfaces, change slowly in space (adjacent points on a surface are not at random depths, for instance). Standard regularization (*1–3*), on which many examples of the early vision algorithms are based, captures those smoothness properties well. The physical properties of surfaces, however, are smooth almost everywhere, but not at discontinuities. Reliable detection of discontinuities of the physical properties of surfaces is critical for a vision system, since discontinuities are often the most important locations in a scene: depth discontinuities, for example, normally correspond to the boundaries of an object. Thus, the output of each vision module has to be smoothed and interpolated (that is, "filled-in"), since it is noisy and often sparse; at the same time discontinuities must be detected.

Discontinuities can also be used effectively to fuse information between different visual cues (*4–7*) and the image data [see also (*8–10*)]. For instance, a depth discontinuity usually produces a sharp change of brightness in the image (usually called a brightness edge); and a motion boundary often corresponds to a depth discontinuity (and a brightness edge) in the image. The idea is thus to couple different cues—stereo, motion, texture, color, and motion—to the image data (in particular, to the sharp changes of brightness in the image) through the discontinuities in the physical properties of the surfaces (see Fig. 1) [for early work in this direction, see (*11*)]. The final goal of this approach is to use information from several cues simultaneously to refine the initial estimation of surface discontinuities. In this report we will describe a first step in this direction that combines brightness edges with discontinuities in each of the modules separately.

How can this be done? We have chosen to use the machinery of Markov random fields (MRFs), initially suggested for image processing by Geman and Geman (*12*) [for alternative approaches see (*13–16*)]. Consider the prototypical problem of approximating a surface (f) given sparse and noisy data (depth data), on a regular two-dimensional lattice of sites (Fig. 2). We first define the prior probability of the class of surfaces in which we are interested. The probability of a certain depth at any given site in the lattice depends only upon neighboring sites (the Markov property). Because of the Clifford-Hammersley theorem, the prior probability has the Gibbs form:

$$P(f) = \frac{1}{Z} e^{-U(f)/T} \qquad (1)$$

where Z is a normalization constant, T is a

Artificial Intelligence Laboratory, Massachusetts Institute of Technology, Cambridge, MA 02139.

quantity analogous to temperature in statistical mechanics, and $U(f) = \sum_i U_i(f)$ is an energy function that can be computed as the sum of local contributions from each lattice site i. The energy at each lattice site $U_i(f)$ is, itself, a sum of the potentials, $U_C(f)$, of each site's cliques. A clique is either a single lattice site or a set of lattice sites such that any two sites belonging to it are neighbors of one another (*5, 17*). As a simple example, when the surfaces are expected to be smooth (like a membrane), the prior energy can be given in terms of

$$U_i(f) = \sum_j (f_i - f_j)^2 \quad (2)$$

where j is a neighboring site to i (that is, i and j belong to the same clique).

If a model of the observation process is available (that is, a model of the noise), then one can write the conditional probability $P(g|f)$ of the sparse observation g for any given surface f. Bayes's theorem then allows one to write the posterior distribution:

$$P(f|g) = \frac{1}{Z} e^{-U(f|g)/T} \quad (3)$$

In the example of Eq. 2, we have (for Gaussian noise):

$$U_i(f|g) = \sum_j (f_i - f_j)^2 + \alpha\gamma_i(f_i - g_i)^2 \quad (4)$$

where $\gamma_i = 1$ only where data are available, and otherwise $\gamma_i = 0$. More complicated cases can be handled in a similar manner (*5*).

The maximum of the posterior distribution or other related estimates cannot be computed analytically, but sample distributions with the probability distribution of Eq. 3 can be obtained by means of Monte Carlo techniques such as the Metropolis algorithm (*18*). These algorithms sample the space of possible surfaces according to the probability distribution $P(f|g)$ that is determined by the prior knowledge of the allowed class of surfaces, the model of noise, and the observed data. In our implementation, a highly parallel computer generates a sequence of surfaces from which, for instance, the surface corresponding to the maximum of $P(f|g)$ can be found. This corresponds to finding the global minimum of $U(f|g)$ (simulated annealing is one of the possible techniques). Other criteria can be used: Marroquin (*19*) has shown that the average surface f under the posterior distribution is often a better estimate, which can be obtained more efficiently simply by finding the average value of f at each lattice site.

One of the main attractions of MRF models is that the prior probability distribution can be made to embed more sophisticated assumptions about the world. Geman and Geman (*12*) introduced the idea of another process, the line process, located on the dual lattice (see Fig. 2), and representing explicitly the presence or absence of discontinuities that break the smoothness assumption (Eq. 2). The associated prior energy then becomes:

$$U_i(f,l) = \sum_j (f_i - f_j)^2(1 - l_i^j) + \beta V_C(l_i^j) \quad (5)$$

where l_i^j is a binary line element between site i and j. The term $V_C(l_i^j)$ reflects the fact that certain configurations of the line process are more likely than others to occur. Depth discontinuities are usually themselves continuous, nonintersecting, and rarely isolated points. These properties of physical discontinuities can be enforced locally by defining an appropriate set of energy values $V_C(l_i^j)$ for different configurations of the line process (*5, 12, 17*).

It is possible to extend the energy function of Eq. 5 to accommodate the interaction of more processes and of their discontinuities. In particular, we have extended the energy function to couple several of the early vision modules (depth, motion, texture, and color) to sharp changes of brightness in the image. This is a central point in our integration scheme: here we assume that changes of brightness guide the computation of discontinuities in the physical properties of the surface, thereby coupling surface depth, surface orientation, motion, texture, and color each to the image brightness data and to each other. The reason for the primary role of the gradient of brightness, as conjectured

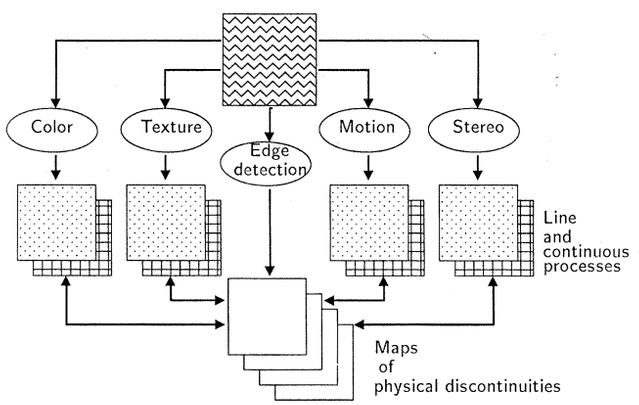

Fig. 1. A sketch of the overall organization of the integration stage (*5, 26*). The outputs of the early visual cues (or algorithms)—stereo, motion, texture, and color—are coupled to their own line process (the crosses), that is, their discontinuities. They are also coupled to the discontinuities in the surface properties—occluding edges (both extremal edges and blades), orientation discontinuities, specular edges, texture marks (including albedo discontinuities), and shadow edges. The image data, especially the sharp changes in brightness labeled here as edges, are input to the lattices that represent the discontinuities in the physical properties of the surfaces. The brightness edges may be completed before integration (in some cases this may lead to "subjective contours") by the equivalent of a higher order MRF that reflects long-range constraints of colinearity and continuation and even hypotheses from the recognition stage, which is then expected to use the set of discontinuities at the top as its main input. Our present implementation does not couple the different types of physical discontinuities: sharp changes in brightness are directly coupled to the line processes of each of the cues. The individual modules are therefore integrated with each other only indirectly, through the brightness edges.

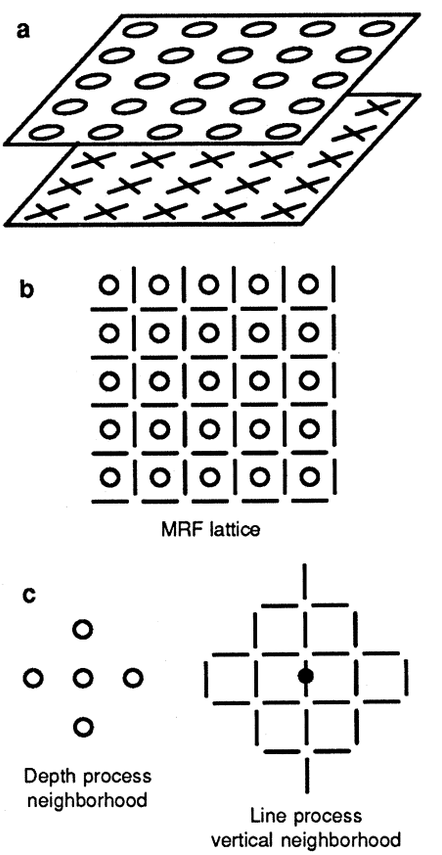

Fig. 2. (**a**) Coupled MRF lattices: the circles represent the continuous process (depth, motion, color, or texture) and the crosses [the lines in (**b**)] represent the associated line process, that is, the discontinuities. The neighborhoods of the continuous process and of the line process are shown in (**c**). The cost of an isolated line process is much higher than that of a continuous line.

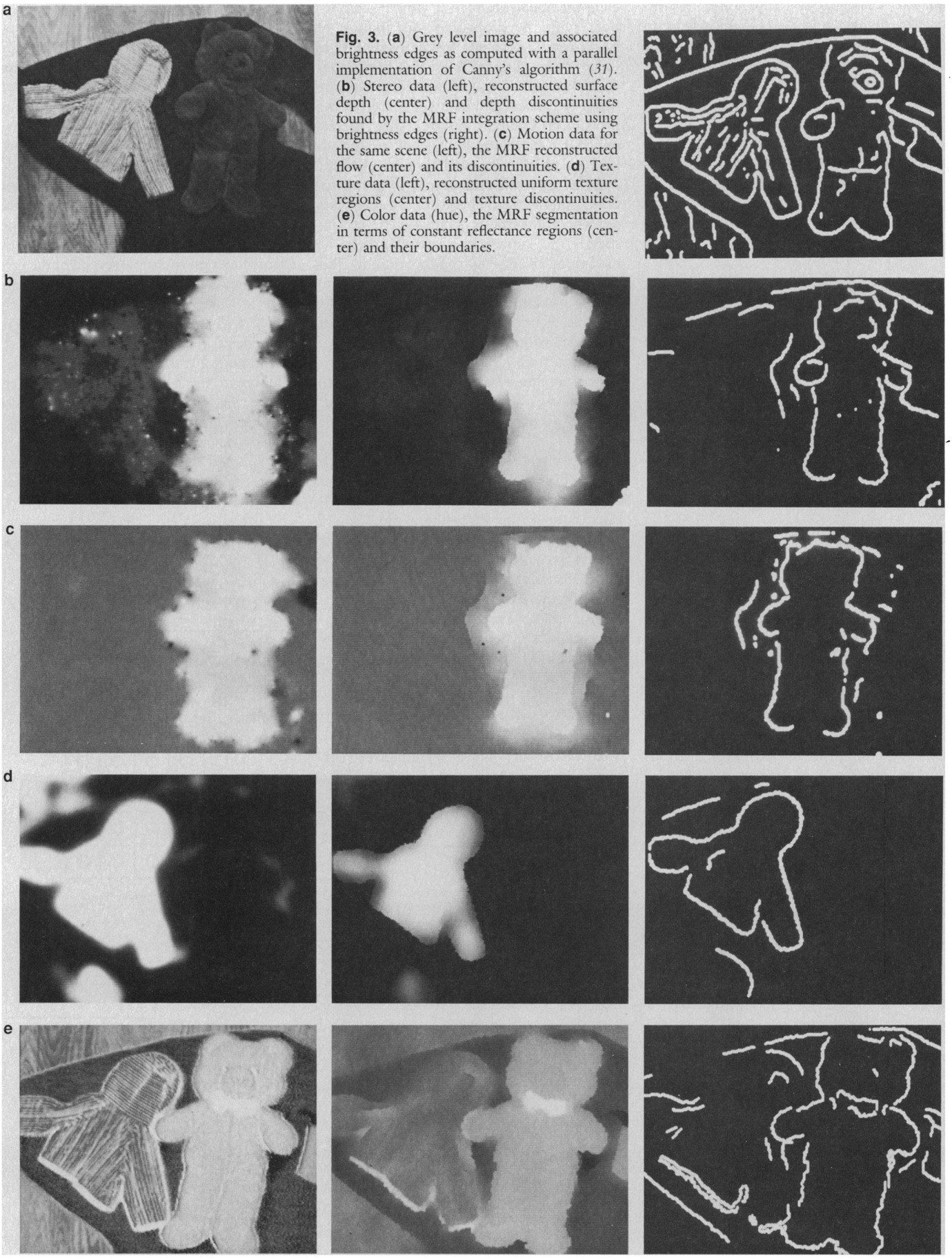

Fig. 3. (**a**) Grey level image and associated brightness edges as computed with a parallel implementation of Canny's algorithm (*31*). (**b**) Stereo data (left), reconstructed surface depth (center) and depth discontinuities found by the MRF integration scheme using brightness edges (right). (**c**) Motion data for the same scene (left), the MRF reconstructed flow (center) and its discontinuities. (**d**) Texture data (left), reconstructed uniform texture regions (center) and texture discontinuities. (**e**) Color data (hue), the MRF segmentation in terms of constant reflectance regions (center) and their boundaries.

here, is that changes in surface properties usually produce large brightness gradients in the image.

The coupling to high brightness gradients may be done by replacing the term $V_C(l_i^j)$ in the last equation with the term:

$$V(l,b) = g(b_i^j, l_i^j) \quad (6)$$

with b_i^j representing a measure of the strength of the brightness gradient (that is, of a brightness edge) between site i and j. The term g has the effect of modifying the probability of the line process configuration depending on the brightness edge data [for instance, $g(b_i^j, l_i^j) = b_i^j(1 - l_i^j)$]. This term facilitates formation of discontinuities (that is, $l_i^j = 1$) at the locations of sharp brightness changes, without restricting them only to brightness edges. High values of the brightness gradient (together with image data in the neighborhood) activate with different probabilities the different types of surface discontinuities (see Fig. 1) which, in turn, are coupled to the output of stereo, motion, color, texture, and possibly other early vision algorithms.

We have been using the MRF machinery with prior energies like that given in Eqs. 5 and 6 (see also Fig. 1) to integrate edge brightness data with stereo, motion, color, and texture information on the MIT Vision Machine System. The system consists of a two-camera eye-head input device and a 16K Connection Machine. All the early vision algorithms—edge detection, stereo, motion, color, and texture—as well as the MRF algorithm, now run on the Connection Machine several hundred times faster than on a conventional machine. The results of integrating brightness edges with a parallel stereo algorithm (*20*) are shown in Fig. 3. In a similar way, the optical flow and its boundary from the same scene are computed from motion data (*21*) and brightness edges (*5, 6, 22, 23*). Simple examples of a similar integration performed with texture and color data are shown in Fig. 3, d and e. The texture algorithm is a greatly simplified parallel version of the texture algorithm developed by Voorhees and Poggio (*24*). It measures the level density of "blobs" extracted from the image through a filtering process involving center-surround filters with appropriate size and threshold. The color algorithm provides a local measure of hue, $H = R/(R + G)$, where R and G are the measurements in the red and green channels, respectively, of a digital color camera. Under certain conditions [A. C. Hurlbert, see (*25*)], this ratio is independent of illumination and three-dimensional (3-D) shape. An MRF model that enforces local constancy of the hue H uses these dense but noisy data to segment the image into regions of different constant reflectance (*26*). The coupling with brightness edges facilitates finding the boundaries: usually sharp changes in the ratio H correspond to a subset of the brightness edges.

The union of the discontinuities in depth, motion, and texture for the scene of Fig. 3 gives a "cartoon" of the original scene. Notice that this "cartoon" represents discontinuities in the physical properties of 3-D surfaces that are well defined, whereas brightness "discontinuities" are not well defined in terms of surface properties. Our integration algorithm achieves a preliminary classification of the edges in the image, in terms of their physical origin. A more complete classification may be achieved by implementing the full scheme of Fig. 1; the lattices at the top classify the different types of discontinuities in the scene: depth discontinuities, orientation discontinuities, albedo edges, specular edges, and shadow edges. The set of such discontinuities in the various physical processes seems to represent a good set of data for later recognition. In some preliminary experiments we have successfully used a parallel, model-based recognition system (*27*) on the discontinuities (stereo and motion) provided by our MRF scheme (*28*).

Our present implementation represents a subset of the possible interactions shown in Fig. 1, itself only a simplified version of the organization of the likely integration process. As described elsewhere (*5, 26*), the system will be improved in an incremental fashion, including pathways not shown in Fig. 1, such as feedback from the results of integration into the matching stage of the stereo and motion algorithms.

The highly parallel algorithms we have described (*29*) map quite naturally onto an architecture such as the Connection Machine, which consists of 64K simple one-bit processors with local and global connection capabilities. The same algorithms also map onto very large scale integration (VLSI) architectures of fully analog elements (we have successfully experimented with a version of Eqs. 5 and 6, in which l is a continuous variable), mixed analog and digital components and purely digital processors (similar to a much simplified and specialized Connection Machine).

A plausible organization of visual integration as sketched in Fig. 1 may be found ultimately by theory and by computer experiments of the type described here. We believe that psychophysical and physiological data about the integration stage in the mammalian visual system may be helpful in guiding our theoretical and computational work. The system described here has already triggered a series of psychophysical experiments in order to establish whether and how brightness edges aid human computation of surface discontinuities (*30*).

REFERENCES AND NOTES

1. T. Poggio and V. Torre, *A.I. Memo No. 773, C.B.I.P. Paper No. 001* (Artificial Intelligence Laboratory, Massachusetts Institute of Technology, Cambridge, 1984).
2. M. Bertero, T. Poggio, V. Torre, *A.I. Memo No. 924* (Artificial Intelligence Laboratory, Massachusetts Institute of Technology, Cambridge, 1987), also *Proc. IEEE*, in press.
3. T. Poggio, V. Torre, C. Koch, *Nature* **317**, 314 (1985).
4. T. Poggio, *Working Paper No. 285* (Artificial Intelligence Laboratory, Massachusetts Institute of Technology, Cambridge, 1985).
5. E. B. Gamble and T. Poggio, *A.I. Memo No. 970* (Artificial Intelligence Laboratory, Massachusetts Institute of Technology, Cambridge, 1987).
6. J. Hutchinson, C. Koch, J. Luo, C. Mead, *IEEE Computer Magazine* **21**, 52 (March 1988).
7. T. Poggio *et al.*, in *Proceedings: Image Understanding Workshop*, Los Angeles, February 1987 (Morgan Kaufmann, San Mateo, CA, 1987), pp. 41–54.
8. P. B. Chou and C. M. Brown, in *Proceedings: Image Understanding Workshop*, Los Angeles, February 1987 (Morgan Kaufmann, San Mateo, CA, 1987), pp. 663–670.
9. P. B. Chou and C. M. Brown, in *Proceedings: International Joint Conference on Artificial Intelligence*, Milan, August 1987 (Morgan Kaufmann, San Mateo, CA, 1987), pp. 779–782.
10. P. B. Chou and C. M. Brown, in *Proceedings: Image Understanding Workshop*, Cambridge, April 1988, (Morgan Kaufmann, San Mateo, CA, 1988), pp. 214–221.
11. H. G. Barrow and J. M. Tenenbaum, in *Computer Vision Systems*, A. R. Hanson and E. M. Riseman, Eds. (Academic Press, New York, 1978), pp. 3–26.
12. S. Geman and D. Geman, *IEEE Trans. Pattern Anal. Mach. Intell.* **PAMI-6**, 721 (1984).
13. W. Hoff and N. Ahuja, in *Proceedings of the International Conference on Computer Vision*, London, June 1987 (IEEE, Washington, DC, 1987), pp. 284–294.
14. A. Blake and A. Zisserman, *Visual Reconstruction* (MIT Press, Cambridge, MA, 1987).
15. J. Aloimonos and C. M. Brown, in *Advances in Computer Vision*, C. Brown, Ed. (Erlbaum, Hillsdale, NJ, 1987), pp. 115–163.
16. F. S. Cohen and D. B. Cooper, in *Proceedings of SPIE Conference on Advances in Intelligent Robotics Systems*, Cambridge, MA, November 1983 (SPIE, the International Society for Optical Engineering, Bellingham, WA, 1983).
17. J. L. Marroquin, S. Mitter, T. Poggio, in *Proceedings: Image Understanding Workshop*, L. Baumann, Ed., Miami Beach, FL, December 1985 (Scientific Applications International Corporation, San Diego, CA, 1985), pp. 293–309.
18. N. Metropolis, A. Rosenbluth, M. Rosenbluth, A. Teller, E. Teller, *J. Phys. Chem.* **21**, 1087 (1953).
19. J. L. Marroquin, *Probabilistic Solution of Inverse Problems*, thesis, Massachusetts Institute of Technology (1985).
20. M. Drumheller and T. Poggio, in *Proceedings of IEEE Conference on Robotics and Automation* (IEEE, Washington, DC, 1986), pp. 1439–1448.
21. J. J. Little, H. H. Bülthoff, T. Poggio, in *Proceedings: Image Understanding Workshop*, Los Angeles, February 1987 (Morgan Kaufmann, San Mateo, CA, 1987), pp. 915–920.
22. D. W. Murray and B. F. Buxton, *IEEE Trans. Pattern Anal. Mach. Intell.* **PAMI-9** (no. 2), 220 (1987).
23. A. L. Yuille, *A.I. Memo No. 987* (Artificial Intelligence Laboratory, Massachusetts Institute of Technology, Cambridge 1987).
24. H. Voorhees and T. Poggio, *Nature* **333**, 364 (1988).
25. T. Poggio *et al.*, in *Proceedings: Image Understanding Workshop*, L. Baumann, Ed., Miami Beach, FL, December 1985 (Scientific Applications Interna-

tional Corporation, San Diego, CA, 1985), pp. 25–39.
26. T. Poggio *et al.*, in *Proceedings: Image Understanding Workshop*, Cambridge, April 1988 (Morgan Kaufmann, San Mateo, CA, 1988), pp. 1–12.
27. T. A. Cass, in *ibid.*, pp. 640–650.
28. We have exploited the labeling of discontinuities (E. B. Gamble, D. Geiger, T. Poggio, D. Weinshall, in preparation) in recognition experiments. In addition, our integration scheme allows us to segment the scene into different depth planes, for instance, thereby considerably reducing the combinatorics of model-based recognition.
29. Our formulation of the integration problem in terms of MRF does not imply that the algorithms are necessarily stochastic. Deterministic approximations to the more general stochastic schemes may work quite well, especially in situations where redundant and contradictory data from several sources effectively set the initial state of the system close to the solution. We have, in fact, found that gradient descent in the space of the depth and the line process often works quite well. We routinely use a mixed deterministic and stochastic strategy (*17*) in which the continuous (depth) process is deterministically updated while the line process is updated stochastically. Other strategies may also be effective (*8*), such as space-variant filtering, for instance, coupled with edge detection. In addition, time-dependent schedules of the coupling parameters can be useful. They are somewhat similar to simulated annealing, which can also be effectively used, though it is quite slow.
30. H. H. Bülthoff, personal communication.
31. J. F. Canny, *IEEE Trans. Pattern Anal. Mach. Intell.* **PAMI-8** (no. 6), 679 (1986).
32. This report describes research done within the Artificial Intelligence Laboratory. Support for the A. I. Laboratory's artificial intelligence research is provided by the Advanced Research Projects Agency of the Department of Defense under Army contract DACA76-85-C-0010 and in part under Office of Naval Research (ONR) contract N00014-85-K-0124. Support for this research is also provided by a grant from ONR, Engineering Psychology Division, and by a gift from the Artificial Intelligence Center of Hughes Aircraft Corporation to T. Poggio.

4 May 1988; accepted 12 August 1988

Earthquake-Caused Coastal Uplift and Its Effects on Rocky Intertidal Kelp Communities

JUAN CARLOS CASTILLA

The coastal uplift (approximately 40 to 60 centimeters) associated with the Chilean earthquake of 3 March 1985 caused extensive mortality of intertidal organisms at the Estación Costera de Investigaciones Marinas, Las Cruces. The kelp belt of the laminarian *Lessonia nigrescens* was particularly affected. Most of the primary space liberated at the upper border of this belt was invaded by species of barnacles, which showed an opportunistic colonization strategy. Drastic modifications in the environment such as coastal uplift, subsidence, or the effects of the El Niño phenomenon are characteristic of the southern Pacific. Modifications in the marine ecosystem that generate catastrophic and widespread mortalities of intertidal organisms can affect species composition, diversity, or local biogeography.

ON 3 MARCH 1985 AT 19:47 A major earthquake, with a surface wave magnitude of 7.8, occurred in central Chile (*1*). The seismic wave originated in the sea bed 40 km west of the coastal town of Algarrobo (33°20′S, 71°40′W) at a depth of approximately 15 km (*2*). The average horizontal displacements in coastal zones were in a northwest direction and of magnitude approximately 25 cm (*3*). Studies on the vertical component of deformation suggest a mean continental uplift of about 33 cm. Maximum uplifts of approximately 45 to 50 cm were observed in coastal areas, such as El Quisco. The coastal marine station (ECIM) of the Pontificia Universidad Católica de Chile (*4*), located on a 500-m stretch of exposed rocky shore at Las Cruces, is 15 to 20 km from both El Quisco and Algarrobo. The seismic wave caused both horizontal and vertical coastal displacements (*3*) at ECIM. I independently checked rocky shore uplifts at ECIM, using previously known fixed benchmarks that were leveled and referred to the extreme low water spring (ELWS) (*5*). The uplifts (Table 1) found at ECIM, about 44 to 59 cm, were roughly within the range determined by Instituto Geográfico Militar (*3*).

It is well established that the zonation patterns of intertidal organisms are determined by biotic and abiotic factors (*6–8*). Among the latter, desiccation and temperature stress can play key roles determining the upper limit of sessile organisms. Hence, in Chile, even under normal weather conditions during ELWS tides at around noontime on sunny days, intertidal macroalgae have been observed to die (bleaching) (*9*). Moreover, substantial modification of intertidal landscapes has been documented (*10, 11*) as a result of increases in seawater temperature. Similarly, coastal uplifts or subsidences resulting from earthquakes or nuclear testing have modified the intertidal zonation patterns or induced mortalities among sessile or mobile species (*12–15*).

Since 1974 the zonation and dynamics of the central Chile rocky intertidal shore have been studied (*16, 17*). Immediately before the March 1985 earthquake I was engaged in an intertidal research program at Las Cruces (*18*). Transects had been made randomly at selected sites, and species composition, primary space, percent coverage, and the change through time in biomass of the macroalga *Lessonia nigrescens* were assessed (*19*). The first two field surveys were conducted on 9 to 10 February and 5 to 8 March 1985. I report here on the effects of the coastal uplift on ECIM rocky shore communities and particularly on the structure and dynamics of the lower rocky shore fringe, the so-called *L. nigrescens* belt (*9, 16, 20*).

Six 1-m-wide transects in the *L. nigrescens* kelp zone, extending 2.5 m from their intertidal upper to lower limit and 3 to 7 m apart, were randomly chosen (*21*). Vertical differences between the lower and upper limits of the belts were 1 to 1.55 m. Each belt, identified by means of poxy putty marks, was divided vertically into five 0.5-m plots (1-m horizontal axis, 0.5-m vertical axis). Plots A (upper limit) to E (lower limit) were sampled 8 to 11 times during the 36-month study. The maximum holdfast diameter (*d*) of each *L. nigrescens* plant within each plot was recorded and the biomass was calculated (*22*).

Figure 1 shows the change in the *L. nigrescens* biomass with time. In the upper plots, A and B, the biomass before the earthquake was about 15 kg m^{-2}, wet weight; this was considered the normal pattern (*23*). A significant decrease in biomass, accompanied by a change in the color of the plants from brown to yellow and the subsequent mortality of the stipes and holdfasts, was evident toward the end of 1985. By February–March 1986 all plants had disappeared from the upper plots. No recolonization has been observed up to February 1988. The biomass record for the middle plot, C, was similar, but the biomass decrease was obvious only in early 1986. By February 1987 almost all plants had disappeared from this plot as well, and no recolonization has since been observed. Plots D and E, the lower plots, behaved differently. At plot D a drastic decrease in *L. nigrescens* biomass was observed in early 1986 (*23*) (about 6 kg m^{-2} by February 1987), but by February 1988 the biomass had increased to about 15 kg m^{-2}. Plot E showed comparatively less change in *L. nigrescens* biomass, with values between 20 and 33 kg m^{-2}. In plot F (not part of the original study because the kelp was absent) *L. nigrescens* was abun-

Estación Costera de Investigaciones Marinas, Facultad de Ciencias Biológicas, Pontificia Universidad Católica de Chile, Casilla 114-D, Santiago, Chile.